Research Journal of
Applied Science
MEDWELL PUBLICATIONS

Synthesis and Characterizations of Graphene-Like Graphite using Renewable Precursors via. Solution Chemical Technique

[1]Abdulmutolib Olajide Olaoye, [2]Rasheed Segun Lawal, [3]Thomas Ojonugwa Daniel, [4]Sani Muhammad Adam, [5]Muhammad Shefiu Shehu and [6]Mohd Arif Agam
[1]Department of Science Technology, Federal Polytechnic Offa, Offa, Kwara State, Nigeria
[2]Department of Physics and Astronomy, University of Nigeria, Nsukka, Nigeria
[3]Department of Physics/Geology/Geophysics, Alex Ekwueme Federal University, Ndufu-Alike, Ebonyi State, Nigeria
[4]Department of Metallurgical and Materials Engineering, University of Nigeria, Nsukka, Nigeria
[5]Department of Physics, Baze University Abuja, Nigeria
[6]Department of Physics and Chemistry, University Tun Hussein Onn Malaysia, Parit Raja, Malaysia

Key words: Graphene, graphite, graphene-like graphite, composite

Corresponding Author:
Abdulmutolib Olajide Olaoye
Department of Science Technology, Federal Polytechnic Offa, Offa, Kwara State, Nigeria

Page No.: 204-209
Volume: 15, Issue 6, 2020
ISSN: 1815-932x
Research Journal of Applied Sciences

Abstract: Graphene-Like Graphite (GLG) samples were prepared using sand and sugar composite as a precursor. GLG was synthesized using solution chemical technique. The produced composite materials dried at a temperature of 120°C in an oven to form a black powder composite material. The structure of the composite was revealed by XRD with narrow diffraction peaks (002) (010) and (004) at 2 = 26.603°, 42.466° and 54.794° with d-spacing of 3.34800 Å, 2.12696 Å and 1.67400 Å, respectively. The average grain size of the material is 599.54Å. Preferential crystal orientations obtained from texture coefficient of the peaks are 2.614, 10.18 and 5.029, respectively. The material shows hexagonal crystal structure with lattice parameters of a = b = 2.4560 and c = 6.6960. SEM with EDX also revealed the morphological and elemental composition of the samples. The SEM images show flake-type GLG and EDX analysis shows the presence of carbon, oxygen, silicon and sulphur at 34.02% at 45.36% at 18.86% at and 1.75% at respectively. The material obtained is potential for solid-state batteries due to flake-type structure that enhance large surface area creation for chemical interaction. This technique may provide economical and environmentally friendly approaches for graphene-like graphite in large scale.

INTRODUCTION

Graphene and related materials have drawn in a large sight of recent interest owing to their uniqueness in terms of structure, physical, chemical, thermal and other properties[1]. Graphene is a Two-Dimensional (2D) hexagonal lattice that consists of a network of sp^2-bonded carbon atoms and represents the "thinnest material" which is stable in its free form Novoselov[2]. Excellent electronic properties[3], thermal conductivity[4-6] and high surface area, combined with unusual mechanical properties and good dispersion performance, make graphene a promising

candidate for structural modification of materials with various applications ranging from electronic devices to biological devices[7, 8].

Single-layer graphenenano-sheets were first obtained by mechanical exfoliation also known as "Scotch-tape" method of bulk graphite and by epitaxial chemical vapor deposition[9]. Various synthesizing method in producing single-layer graphenenano-sheets including chemical vapor deposition cleavage and annealing of single-crystal SiC under ultrahigh vacuum, nevertheless the high energy requirement and low yield has limited the potential application of single-layer graphenenano-sheets[10].

Chemical reduction is considered as a potential approach in synthesizing large volume and low cost of Graphe Nenano Sheets (GNS)[11, 12]. The environmental friendly and mass production of the aforementioned method is vital for commercial industrial production, beside the abilities to fabricate different variants of graphene by chemical modifications[13].

In this report, we demonstrate that Graphene-Like Graphite (GLG) material can be produced in large scale using renewable precursors. To the best of our knowledge, this is the first paper reporting the use of renewable precursors to synthesize graphene-like graphite for mass production.

MATERIALS AND METHODS

Experimental: River sand was collected from Enji River at Offa, Kwara state, Nigeria. All the chemicals used were of analytical grade. The sulfuric acid, nitric acid and activated charcoal were purchased from LABTRADE, Ilorin, Nigeria while table sugar was obtained from Owode Market Offa. The river sand was washed, rinsed dried and filtered before treated with Nitric acid to eliminate the organic materials present.

Synthesis of graphene-like graphite: A 342 g of sugar crystals were dissolved into 1 L of distilled water to make 1 m of sugar solution. The river sand was treated with 0.1 m Nitric acid in order to remove impurities, later washed with deionized water anddried at 100°C. The sugar solution of 1 m concentration and 40 g of sandwith average grain size of 0.22 mm was stirred continuously for 5 h with magnetic stirrer at 85°C. The mixture was later dried and placed in the crucible thatwas covered with activated charcoal and heated for 6 h in muffle furnace. The obtained powder (white in color) was treated with 45 mL of concentrated sulfuric acid and washed with de-ionized water. The powder was let todry in an oven at 120°C for 3 h that later turned to black in color. Figure 1 shows the formation of GLG.

Characterization of GLG: The X-Ray Diffraction (XRD) measurement was carried out with EMPYREAM Diffracto meter with Cu Kα radiation (Kα 1.540560Å) and X-ray power of 45 kV/40 mA at a scan rate of 5° min^{-1}. XRD pattern was obtained using Origin Pro 2018 software with FWHM for peaks estimated using a Gaussian function. Scientific graphing analysis software was used to analyze the result and phase identification was done using the Inorganic Crystal Structure Data (ICSD) pattern[14]. The Scanning Electron Microscope (SEM) (Hitachi X650) equipped with Energy Dispersive Spectroscopy to reveal the morphological features and elemental composition of GLG structure. The instrument operated at a voltage of 20 kV while the image was captured using voltage acceleration of 5 kV to reduce charge accumulation to the sample.

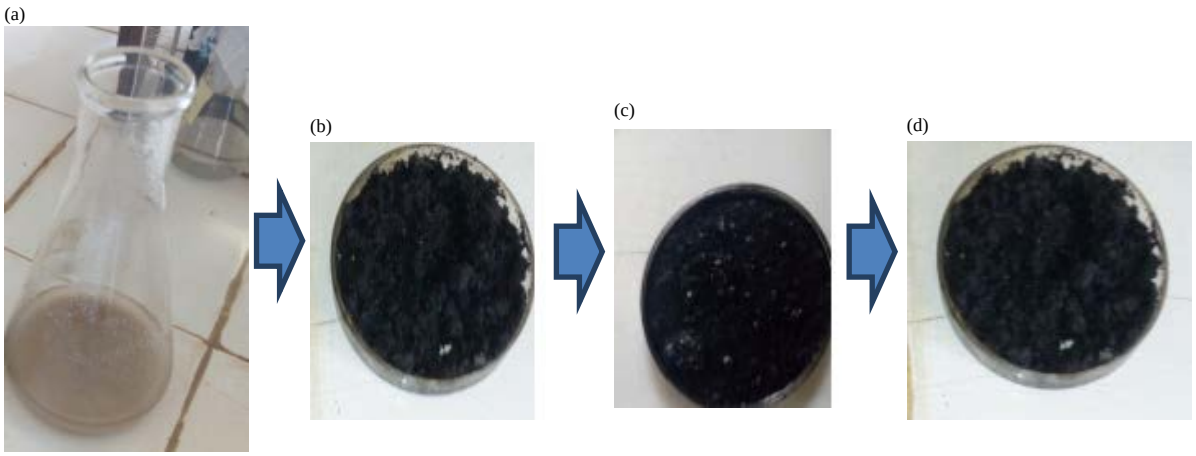

Fig. 1(a-d): Steps in the formation of GLG (a) sample powder before heating (b) The 1 h heat treatment (c) The 2 h heat treatment and (d) The 3 h heat treatment

RESULTS AND DISCUSSION

Structural analysis: The XRD pattern as in Fig. 2 of GLG exhibited the characteristic peaks at 2θ = 26.603°, 42.466° and 54.794° corresponding to (002), (010) and (004) reflection, respectively which is in agreement with Cheng *et al*.[15],. The material also shows the presence of Quartz and Anatase. Quantz: (010), (110), (111), (112), (121) (203) and (104) at corresponding 2θ = 20.865°, 36.557°, 40.304°, 50.155°, 59.980°, 68.164° and 73.487°, respectively while Anatase is presented with XRD peak pattern of (112) at 2θ = 39.164°. Table 1 shows the summary of XRD analysis for GLG. The lattice parameters were calculated to be a = b = 2.4560 and c = 6.6960.

The lattice parameters a = b and c for hexagonal crystal structure of GLG was calculated from the observed values of 2θ using d values (interplanar spacing) for the hexagonal structure:

$$\frac{1}{d^2}=\frac{4}{3}\left(\frac{h^2+hk+k^2}{a^2}\right)+\frac{I^2}{c^2} \quad (1)$$

where, d is inter atomic spacing which can be calculated using Eq. 2:

$$d=\frac{\lambda}{2\sin\theta} \quad (2)$$

a and c can be calculated using Eq. 3 and 4, respectively[16]:

$$a=\frac{\lambda}{\sqrt{3}\sin\theta}\sqrt{h^2+hk+k^2} \quad (3)$$

$$c=\frac{\lambda}{2\sin\theta}l \quad (4)$$

The ratio of the hexagonal height "c" total the basal side "a"is called axial ratio by Eq. 5[8]:

$$\text{axial ratio}=\frac{c}{a} \quad (5)$$

The ideal axial ratio of Hexagonal Close-Packed crystal structure (HCP) is 1.633. The axial ratio for this material was evaluated to be 2.726 which indicates that the atoms of the material is elongated along c-axis which is its stiffness depends along that direction. This is a measure to show the anisotropy of the HCP crystal lattice[17].

The pattern obtained has been indexed as a hexagonal unit cell with reference code (96-900-8570).

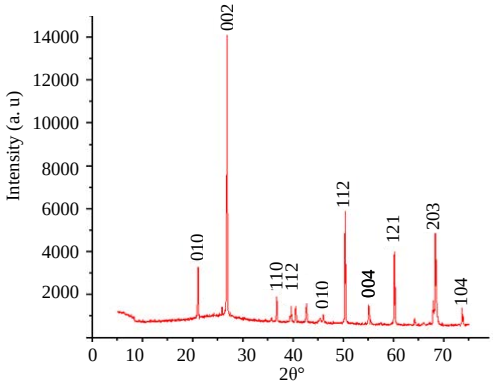

Fig. 2: XRD pattern of GLG; Brown sand

The crystal size (D) has been calculated by Debye-Scherrer formula using the raw data from XRD pattern[18].

The average crystal size was calculated to be 599.54. The formula is given in Eq. 6 and the calculated values are shown in Table 1:

$$D=\frac{k\lambda}{\beta\cos\theta} \quad (6)$$

Where k is the crystallite shape factor (constant) with approximation to 0.9, D is the crystal size (in), λ is wavelength (1.54060), β is Full Width at Half Maximum (FWHM in radian) and θ is the Bragg diffraction angle[19]. The preferential crystal orientation can be obtained from the texture coefficient T_c which is given by the Eq. 7[20]:

$$T_{c(hkl)}=\frac{I_{(hkl)}}{I_{r(hkl)}}\left(\frac{1}{n}\sum\frac{I_{(hkl)}}{I_{r(hkl)}}\right)^{-1} \quad (7)$$

where, $T_{c(hkl)}$ is the texture coefficient, $I_{(hkl)}$ is the XRD intensity, n is the number of diffraction peaks considered and $I_{r(hkl)}$ is the standard intensity of the plane which is taken from reference data[21].

If $T_{c(hkl)}$~1 for all the considered planes, the particles are randomly oriented. It can be observed from Table 1 that $T_{c(hkl)}$ values from planes (002), (010) and (004) are more than unitary which indicates there is an abundance of grain formed along those planes[17]. This also indicates a higher degree of preferred orientation along those planes The deviation in the $T_{c(hkl)}$ from unitary will correspond to change in atomic densitiesof (002) (010) and (004). Thus, the texture analysis of GLG, indicates that the material is highly textured along (010) plane[22].

The microstrain ε induced in the powder due to crystal imperfection and distortion was calculated by Williamson-Hall Eq. 8 which is shown in Table 1:

$$\varepsilon=\frac{\beta\cos\theta}{4} \quad (8)$$

Table 1: hkl, FWHM, grain size, Microstrain, dislocation density and texture coefficient

hkl	d-spacing (Å)	FWHM×10^3 (Radian)	Grain size (Å)	Microstrain	Dislocation density×10^{-6}	Texture coefficient
002	3.34800	2.68	516.20	0.225	3.753	2.61
010	2.12696	1.79	774.51	0.225	1.667	10.18
004	1.67400	2.73	507.91	0.225	3.876	5.02

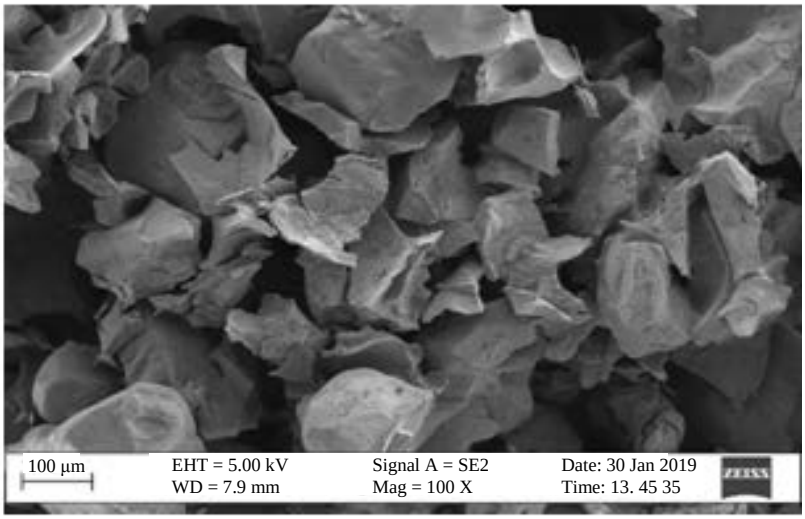

Fig. 3: SEM image of GLG at 100x magnification

The dislocation density (δ) as given by Williamson and Smallman's formula shown in Table 1, represents the amount of defects in the powder which is determined by Eq. 9. The larger D and smaller FWHM values indicate better crystallization of the particle[14]:

$$\delta = \frac{1}{D} \tag{9}$$

From Table 1, it can be observed that plane (010) will have good crystallization particles. In evaluating the degree of crystallinity of this material from XRD reflections, the integrated intensity from diffraction peak is proportional to the material density[23]. The crystallinity P of the material will be obtained with Eq. 10:

$$P = \frac{A}{A_r} \times 100\% \tag{10}$$

Where:
A = The area of crystalline peaks
A_r = The area of all peaks for crystalline and amorphous

The degree of crystallinity was calculated to be 66.67% which indicates that the material is more crystal than amorphous.

Morphological and elemental analysis: The microstructure and energy spectrum analysis data on the intensity of GLG are shown in Figure 3 and 4, respectively. The SEM image of GLG with 100x magnification presents thestructure of flake type GLG. Furthermore, the EDX spectra of GLG is shown in Fig. 3.

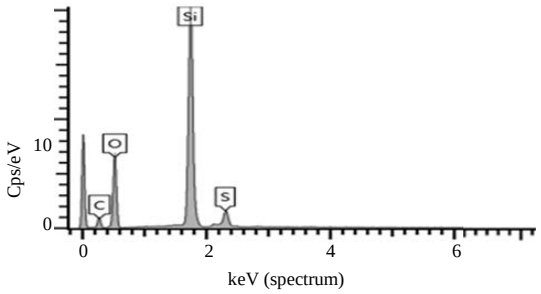

Fig. 4: EDX Spectra of GLG

The EDX spectra data of GLG are measured at a voltage of 15 kV. The GLG EDX spectra data show that the carbon and oxygen atoms have the energy captured by each detector at 0.15 and 0.25 keV, respectively. This material consist of impurities such as Silicon (Si) and Sulphur (S) which appear probably due to the sand and conc. Sulphuric acid used. Table 2 shows the atomic percentage of each element present.

Optical analysis: The UV visible spectrum of the sample is as shown in Fig. 5 and 6. The sample absorbs the

Table 2: Element and atomic percentage

Elements	Atomic %
C	34.02
O	45.36
Si	18.86
S	1.75

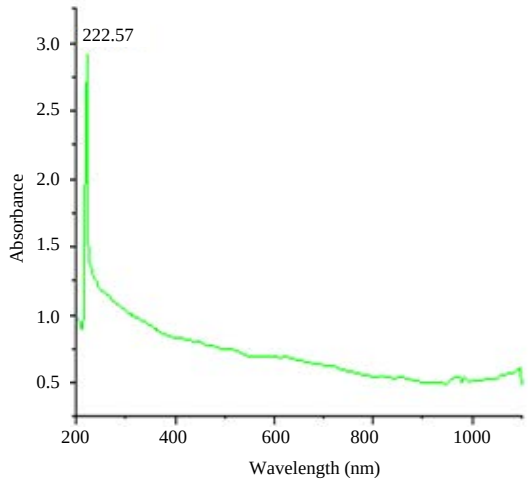

Fig. 5: Absorbance against wavelength (absorbance)

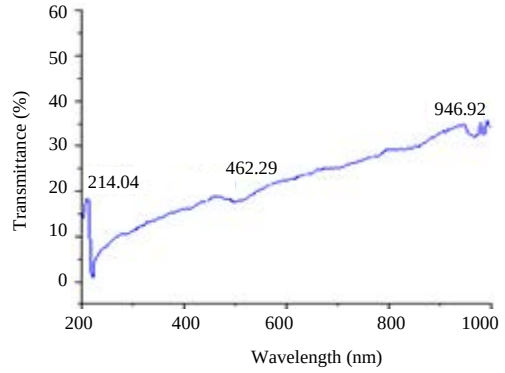

Fig. 6: Transmittance against wavelength

radiations in the UV range up to 222.57 nm. The graphene composite material is absorbed through visible spectrum radiations.

The absorption and the transmission spectra of graphene composite material are shown in Fig. 5 and 6, respectively. It can be seen that the absorbance of the graphene composite material is high at short wavelengths (λ<380 nm) and low at long wavelengths (λ>380 nm). The spectrum shows increased absorbance below ~225 nm but decreased absorbance trend extending beyond 1000 nm of wavelength. The peak maxima can be attributed to π-conjugation partially restored within the aromatic C-C graphene in consistency with earlier reports[24]. The absorption is in ultraviolet range[17]. π-π plasmon bonds is anisotropic optical property of graphite and graphene which is collective π-electron in the ultraviolet frequency region. Plasmon absorption in the ultraviolent region is extremely strong for all carbon materials such as graphite, graphene, carbon nanotubes and amorphous carbon which have been studied for visible and near infrared absorption based applications[25]. In Fig. 6, it is shown that the transmission of graphene composite material is high over large wavelengths. Graphene composite material exhibits a high average transmittance (~50.54%) in the visible region. This suggests that the produced graphene-like material indicates a good optical quality due to low scatter or absorption losses[15].

CONCLUSION

Graphene-like graphite was successfully synthesized from renewable precursors. GLG was prepared by chemical solution method when sand and table sugar were used as starting precursors. The XRD pattern obtained confirmed the formation of hexagonal GLG with secondary phases of quartz and anatase. The XRD studies of GLG revealed that the average grain size which was calculated by Debye-Scherrer formula is 599.54. The highest texture coefficient was found in (010) plane. Also, the microstrain contribution has been analyzed by using Williamson and Hall method which was found to be the same for (002) (010) and (004) planes. The characterization of SEM-EDX show that the GLG internal structure is of flake type and also revealed the elemental composition of the material. This study provides a new approach which can be used to produce graphene base composite material that will be cost effective and large-scale production.

ACKNOWLEDGEMENTS

The researchers acknowledge the Department of Science Laboratory Technology, Federal Polytechnic Offa, Kwara State, Nigeria for making their laboratories available for this research.

REFERENCES

01. Chae, H.K., D.Y. Siberio-Perez, J. Kim, Y. Go and M. Eddaoudi *et alJune 27, 2020*., 2004. A route to high surface area, porosity and inclusion of large molecules in crystals. Nature, 427: 523-527.
02. Novoselov, K.S., A.K. Geim, S.V. Morozov, D. Jiang and Y. Zhang *et al.*, 2004. Electric field effect in atomically thin carbon films. Science, 306: 666-669.
03. Stankovich, S., D.A. Dikin, G.H.B. Dommett, K.M. Kohlhaas and E.J. Zimney *et al*., 2006. Graphene-based composite materials. Nature, 442: 282-826.

04. Shahil, K.M. and A.A. Balandin, 2012. Thermal properties of graphene and multilayer graphene: Applications in thermal interface materials. Solid State Commun., 152: 1331-1340.
05. Balandin, A.A., 2011. Thermal properties of graphene and nanostructured carbon materials. Nat. Mater., 10: 569-581.
06. Fugallo, G., A. Cepellotti, L. Paulatto, M. Lazzeri, N. Marzari and F. Mauri, 2014. Thermal conductivity of graphene and graphite: Collective excitations and mean free paths. Nano Lett., 14: 6109-6114.
07. Olumurewa, K.O., B. Olofinjana, O. Fasakin, M.A. Eleruja and E.O.B. Ajayi, 2017. Characterization of high yield graphene oxide synthesized by simplified hummers method. Graphene, 6: 85-98.
08. Cheng, Y., S. Zhou, P. Hu, G. Zhao, Y. Li, X. Zhang and W. Han, 2017. Enhanced mechanical, thermal and electric properties of graphene aerogels via. supercritical ethanol drying and high-temperature thermal reduction. Sci. Rep., 7: 1-11.
09. Zhang, B., J. Song, G. Yang and B. Han, 2014. Large-scale production of high-quality graphene using glucose and ferric chloride. Chem. Sci., 5: 4656-4660.
10. Loryuenyong, V., K. Totepvimarn, P. Eimburanapravat, W. Boonchompoo and A. Buasri, 2013. Preparation and characterization of reduced graphene oxide sheets via water-based exfoliation and reduction methods. Adv. Mater. Sci. Eng., Vol. 2013, 10.1155/2013/923403.
11. De Silva, K.K.H., H.H. Huang, R.K. Joshi and M. Yoshimura, 2017. Chemical reduction of graphene oxide using green reductants. Carbon, 119: 190-199.
12. Ma, Q., J. Song, C. Jin, Z. Li and J. Liu *et al*., 2013. A rapid and easy approach for the reduction of graphene oxide by formamidinesulfinic acid. Carbon, 54: 36-41.
13. Wang, Y., L. Sun and B. Fugetsu, 2012. Thiourea dioxide as a green reductant for the mass production of solution-based graphene. Bull. Chem. Soc. Japan, 85: 1339-1344.
14. Xu, K., J. Liang, A. Woeppel, M.E. Bostian and H. Ding *et al.*, 2019. Electric double-layer gating of two-dimensional field-effect transistors using a single-ion conductor. ACS Applied Mater. Interfaces, 11: 35879-35887.
15. Cheng, Q., Y. Okamoto, N. Tamura, M. Tsuji, S. Maruyama and Y. Matsuo, 2017. Graphene-like-graphite as fast-chargeable and high-capacity anode materials for lithium ion batteries. Sci. Rep., 7: 1-14.
16. Suryanarayana, C. and M.G. Norton, 1998. Practical Aspects of X-Ray Diffraction. In: X-Ray Diffraction, Suryanarayana, C. and M.G. Norton (Eds.). Springer, Boston, Massachusetts, pp: 63-94.
17. Banerjee, R., E.A. Sperling, G.B. Thompson, H.L. Fraser, S. Bose and P. Ayyub, 2003. Lattice expansion in nanocrystalline niobium thin films. Applied Phys. Lett., 82: 4250-4252.
18. Saleh, A.T., L.S. Ling and R. Hussain, 2016. Injectable magnesium-doped brushite cement for controlled drug release application. J. Mater. Sci., 51: 7427-7439.
19. Singh, A. and H.L. Vishwakarma, 2015. Study of structural, morphological, optical and electroluminescent properties of undoped ZnO nanorods grown by a simple chemical precipitation. Mater. Sci. Poland, 33: 751-759.
20. Ilican, S., Y. Caglar and M. Caglar, 2008. Preparation and characterization of ZnO thin films deposited by sol-gel spin coating method. J. Optoelectr. Adv. Materials, 10: 2578-2583.
21. Kumar, M., A. Kumar and A.C. Abhyankar, 2015. Influence of texture coefficient on surface morphology and sensing properties of w-doped nanocrystalline tin oxide thin films. ACS Applied Mater. Interfaces, 7: 3571-3580.
22. Williamson, G.K. and R.E. Smallman, 1956. III. Dislocation densities in some annealed and cold-worked metals from measurements on the X-ray debye-scherrer spectrum. Philos. Mag., 1: 34-46.
23. Feng, B., X. Fang, H.X. Wang, W. Dong and Y.C. Li, 2016. The effect of crystallinity on compressive properties of Al-PTFE. Polymers, Vol. 8, 10.3390/polym8100356
24. Paul, H. and D. Mohanta, 2011. Hydrazine reduced exfoliated graphene/graphene oxide layers and magnetoconductance measurements of Ge-supported graphene layers. Applied Phys. A, 103: 395-402.
25. Cheung, W., M. Patel, Y. Ma, Y. Chen and Q. Xie *et al.*, 2016. $\bar{x}$ -Plasmon absorption of carbon nanotubes for the selective and sensitive detection of Fe 3+ ions. Chem. Sci., 7: 5192-5199.